JACS
JOURNAL OF THE AMERICAN CHEMICAL SOCIETY

Communication

pubs.acs.org/JACS

Synthesis of Platinum Nanotubes and Nanorings via Simultaneous Metal Alloying and Etching

Zhiqi Huang,[†,‡] David Raciti,[§] Shengnan Yu,[†] Lei Zhang,[†] Lin Deng,[¶] Jie He,[‡] Yijing Liu,[‡] Niveeen M. Khashab,[¶] Chao Wang,[§] Jinlong Gong,*[,†] and Zhihong Nie*[,‡]

[†]Key Laboratory for Green Chemical Technology of Ministry of Education, School of Chemical Engineering and Technology, Tianjin University, Collaborative Innovation Center of Chemical Science and Engineering, Tianjin 300072, China

[‡]Department of Chemistry and Biochemistry, University of Maryland, College Park, Maryland 20742, United States

[§]Department of Chemical and Biomolecular Engineering, John Hopkins University, Baltimore, Maryland 21218, United States

[¶]Smart Hybrid Materials laboratory (SHMs), Advanced Membranes and Porous Materials Center (AMPMC), Physical Sciences and Engineering Division, King Abdullah University of Science and Technology (KAUST), Thuwal 23955, Kingdom of Saudi Arabia

Supporting Information

ABSTRACT: Metallic nanotubes represent a class of hollow nanostructures with unique catalytic properties. However, the wet-chemical synthesis of metallic nanotubes remains a substantial challenge, especially for those with dimensions below 50 nm. This communication describes a simultaneous alloying-etching strategy for the synthesis of Pt nanotubes with open ends by selective etching Au core from coaxial Au/Pt nanorods. This approach can be extended for the preparation of Pt nanorings when Saturn-like Au core/Pt shell nanoparticles are used. The diameter and wall thickness of both nanotubes and nanorings can be readily controlled in the range of 14−37 nm and 2−32 nm, respectively. We further demonstrated that the nanotubes with ultrathin side walls showed superior catalytic performance in oxygen reduction reaction.

Hollow metallic nanoparticles (NPs) exhibit a unique set of features that are different from their solid counterparts, including high surface-to-volume ratio, low density, superior load carrying ability, and tunable optical properties.[1,2] They have shown applications in diverse fields, ranging from catalysis,[3−5] sensing[6] to biomedicine.[7,8] During the past few decades, various synthetic strategies, based on galvanic replacement,[9−11] Kirkendall effect,[12] templating[3,13] or self-templating,[4,14] have been developed for preparing hollow metallic NPs with various architectures (e.g., hollow spheres, boxes, frames, rings). Among them, hollow metallic nanotubes (NTs) are of particular interest due to their unique tubular feature, which uniquely combines the physical and electronic characteristics of one-dimensional and two-dimensional structures.[15] They have shown a variety of promising applications ranging from catalysis to biomedicine. For instance, bare Au NT arrays with a length of 10 μm showed excellent CO oxidation performances comparable to supported Au catalysts.[16] Pt-based NTs with a length of 8 μm were demonstrated as nanomotors that can self-propel at high speed with low level of fuels.[17]

Over the past decades, metallic NTs have been synthesized by templating on porous materials with channels (such as anodized aluminum oxide,[18] polycarbonate membrane[17]) and enlongated nanostructures (such as inorganic nanowires[19,20] and elongated soft materials[21]). The NTs synthesized by these methods usually have lengths from 100 nanometers to several micrometers and wall thicknesses from several nanometers to several tens of nanometers. It is known that the size of nanostructures is crucial to their optical, electronic and catalytic properties and resulting applications. The limited control over tube dimension severely hinders the exploitation of their potential applications in such as catalysis, bioimaging and drug delivery. However, to date, there has been no report on the wet-chemical synthesis of small metallic NTs with a dimension of sub-50 nm.

Here we present a novel strategy to synthesize Pt NTs with sub-50 nm dimensions by selective etching Au core/Pt shell coaxial-like nanorods through a unique simultaneous alloying-etching strategy. These coaxial nanorods used as starting materials were featured by the exposure of both ends of the Au core to surrounding solvent media.[22] Copper ions were employed as etchant to etch and remove the Au cores to produce Pt NTs in organic solvent dimethylformamide (DMF). The same strategy can be used to synthesize Pt nanorings (NRs) when Saturn-like NPs with Au core/Pt shell were used. The diameter and wall thickness of derived NTs (or NRs) can be readily tuned in the range of 14−37 nm (15−30 nm) and 2−25 nm (4−32 nm), respectively. As a demonstration, Pt NTs and NRs with ultrathin shells were used as catalysts for oxygen reduction reaction (ORR). The activity of NTs are 3.6 and 2.6 times higher than that of commercial Pt/C and NRs, respectively. Despite the polycrystalline nature and the large dimensions, the activity reaches 72% of the reported Pt nanocages[3] with well-defined surfaces and smaller dimensions. This method can be extended for the synthesis of other structurally unique hollow nanostructures with different compositions (e.g., oxides), when other anisotropic NPs (e.g., platelets[10]) are used as sacrificial core.

Au core/Pt shell coaxial-like nanorods were synthesized by the preferential deposition of Pt on the side of Au nanorods

Received: February 4, 2016
Published: April 19, 2016

DOI: 10.1021/jacs.6b01328
J. Am. Chem. Soc. 2016, 138, 6332−6335

with a diameter of 14 nm and a length of 40 nm (see detailed synthetic procedures in Supporting Information (SI)).[22] The coaxial-like growth of Pt tubular shell relies on the selective protection of both ends of the nanorods with locally collapsed hydrophobic polystyrene domains in an aqueous growth solution.[23] Figure S1 reveals a coaxial-like construction of nanostructures with the sides of Au nanorod surrounded by a tubular polycrystalline Pt shell and the deprivation of inorganic deposites at both ends of the Au nanorod. These coaxial nanorods were dispersed in DMF with solubilized polystyrene chains serving as stabilizing ligands (Figure S1c). The etching of Au cores was performed by adding appropriate amount of copper chloride and incubating the solution in a 60 °C water bath for 6 h. The products were washed with DMF to remove reactants and polymers and then redispersed in water. Transmission electron microscopy (TEM) images in Figure 1a,b show representative NTs synthesized by this method. The

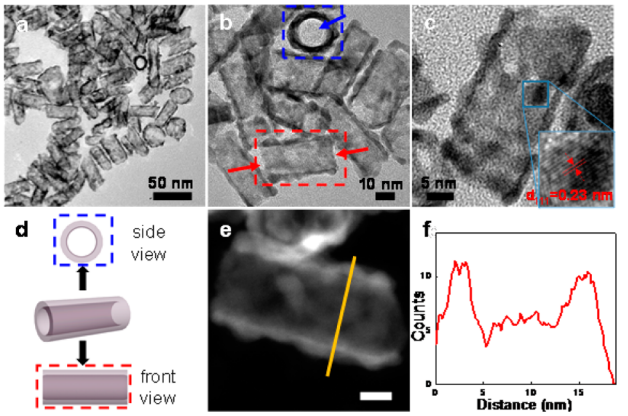

Figure 1. (a and b) TEM images of Pt NTs. Red and blue squares highlight horizontally lying and vertically standing individual NTs, with arrows pointing to the open ends. (c) HRTEM image of an individual Pt NT. Inset is enlarged image of the square area highlighting Pt lattice. (d) Structural model of Pt NT and its front view (corresponding to horizontally lying NT) and side view (corresponding to vertically standing NT). (e) HADDF TEM image of an individual Pt NT. (f) EDS line scan showing the distribution of Pt along yellow line in (e).

NTs have a length of 35.6 ± 1.4 nm and an inner diameter of 13.5 ± 1.2 nm (Figure S2) that are comparable to the dimension of the starting Au nanorod cores. The NTs maintain structural integrity in the presence of hollow interior, and have a mean thickness of 2.0 nm (Figure S3). The NTs are composed of pure Pt, as confirmed by both inductively coupled plasma mass spectrometry (ICP-MS) and TEM EDS analysis (Figure S4). The lattice spacing value of 0.23 nm measured from high resolution TEM (HRTEM) image (Figure 1c) can thus be assigned to Pt(111) facet. Figure 1d shows the structural model of Pt NT from different view angles, which matches well with the horizontally lying and vertically standing NTs highlighted in Figure 1b. The contrast between the edge and middle of the NTs under TEM and high-angle annular dark field TEM (HAADF-TEM, Figure 1e) indicates a typical hollow feature of the nanostructures. The typical double peaks in the elemental line scan along the radial direction further confirm the feature of tubular structures (Figure 1f). Notably, the ends of the NTs are not enclosed by Pt walls, as reflected by the absence of high contrast edges at both ends (red arrows in Figure 1b). The open ends and hollow interior can be more clearly observed from some vertically standing NTs (blue arrows in Figure 1b and Figure S5). We note that the deprivation of inorganic deposites at the ends is *vital* to the access of etchants to the interior Au cores and hence the formation of the NTs. When Au/Pt nanorods with conventional core−shell geometry were used, the same etching process did not lead to the formation of hollow Pt NTs (Figure S6).

Time dependent experiment was carried out to explore the mechanism of etching process. TEM images were taken by quenching the reaction 0.5, 1.5, and 4.5 h after the initiation of etching process (Figure 2a−c). At 0.5 h, the coaxial hybrid

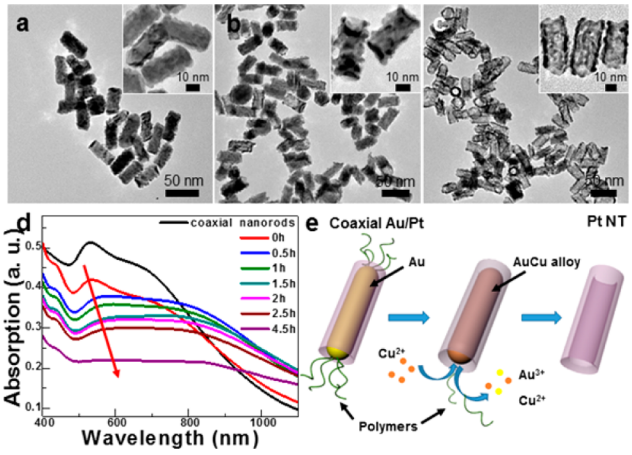

Figure 2. (a−c) TEM images of Au/Pt coaxial nanorods after different etching times: 0.5 h (a), 1.5 h (b), and 3 h (c). (d) Time-dependent UV−vis absorption spectrum of Au−Pt coaxial nanorods during etching process. (e) Proposed simultaneous alloying−etching mechanism for the formation of Pt NTs.

nanorods remained largely intact. At 1.5 h, part of the Au cores was disappeared, indicating the onset of the etching process. Eventually at 4.5 h, all the nanostructures exhibited completely hollow interior. The etching process was accompanied by obvious change in the localized surface plasmon resonance (LSPR), as shown in the UV−vis absorption spectra (Figure 2d). The Au/Pt coaxial nanorods have two absorption peaks at 530 and 700 nm, which correspond to the transversal and longitudinal LSPR of the nanorods, respectively. When $CuCl_2$ was introduced, a new peak at 430 nm corresponding to the absorption of Cu ions appeared and it did not interfere with the absorption of Au structures. The absorption peak at 530 nm gradually red-shifted and weakened in intensity with increasing incubation time, and eventually completely disappeared at 4.5 h. This indicates the slow dissolution of Au cores, which is in accordance with TEM observations.

The formation of NTs constitutes a unique alloying and etching mechanism, which is conceptually different from the conventional copper ions assisted etching process, where copper ions were believed to catalyze the oxidative etching process.[24] As illustrated in Figure 2e, Cu ions were first reduced by DMF[25,26] at elevated temperature (Figure S7) and formed alloys with Au cores.[27] The AuCu alloy cores were then rapidly oxidized by dissolved oxygen at elevated temperature, as alloying with Cu dramatically decreased the stability of Au.[28] Polymers originally tethered to the Au core gradually dissolved into the solvent upon the dissolution of Au. This hypothesis is supported by the following facts. First, intentional introduction of hydrogen peroxide did not lead to the etching of Au core in

DOI: 10.1021/jacs.6b01328
J. Am. Chem. Soc. 2016, 138, 6332−6335

neither water (Figure S8) nor DMF (Figure S9a); addition of hydroxide radical scavenger dimethyl sulfoxide (DMSO) was incapable of preventing the etching (Figure S9b). Thus, the copper ion-catalyzed generation of hydroxide radical should not be responsible for our etching process.[29] Second, the etching process is very sensitive to the reaction temperature: lowering temperature to 30 °C prohibited the etching (Figure S10), as the DMF became less reductive at lower temperature.[26] Third, the amount of copper ions is critical for the etching process. Control experiments were conducted using 0.5 and 2 times the amount of copper ions as etchant, respectively. The alloying of Cu with Au cores was observed in all these cases, as shown by the red-shift of SPR peaks (Figure 2d and Figure S11a,b),[30] whereas the etching only occurred when adequate copper ions were used (Figure 2c and Figure S11c). Insufficient copper ions only led to the formation of coaxial AuCu/Pt hybrid nanorods (Figure S11d), as the stability of AuCu alloy is known to decrease with increasing Cu/Au ratio.[28] Substituting copper with other cations (e.g., Co^{2+}, Ni^{2+}) did not produce Pt NTs, while anion did not affect the etching process (Figure S12). This further confirmed the indispensable role of copper ions.

The shell thickness and inner diameter of Pt NTs can be precisely controlled by using Au/Pt coaxial nanorods with different Pt shell thickness. Figure 3a–c shows Pt NTs with

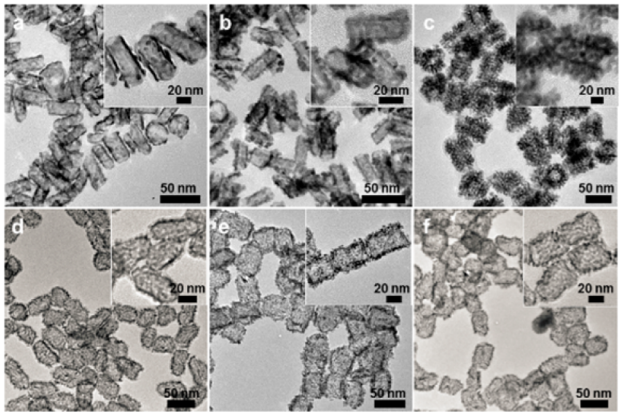

Figure 3. (a–c) TEM images of Pt NTs with different shell thickness: 2 nm (a), 8 nm (b), and 25 nm (c). (d–f) TEM images of Pt NTs with different inner diameter: 20 nm (d), 28 nm (e), and 37 nm (f).

shell thickness increasing from 2 to 25 nm (Figure S13). The initial deposition of Pt formed continuous shell with bumps (Figure 3 a,b), while further growth of Pt led to the formation of hollow urchin-like structures with polycrystalline dendrites.[31] The inner diameter of NTs can be controlled by constructing a sacrificial intermediate Pd layer which can also be alloyed and etched by copper ions (Figure S14). By introducing Pd intermediate layer with different thicknesses, we synthesized NTs with inner diameter ranging from 14 to 37 nm (Figure 1a and Figure 3d–f).

The same method can be employed to synthesize Pt NRs by using Saturn-like Au/Pt hybrid NPs with spherical Au NPs as cores (Figure S15), as illustrated in Figure 4a. Similar to Pt NTs, the derived NRs with thin shell were featured by continuous skeleton decorated with small bumps (Figure 4b,c), while NRs with thick shell showed coral-like morphology (Figure 4d). When starting with Au NPs with different sizes, the inner dimeter of the NRs could be readily tuned from 15 to 30 nm, as shown in Figure 4e–g.

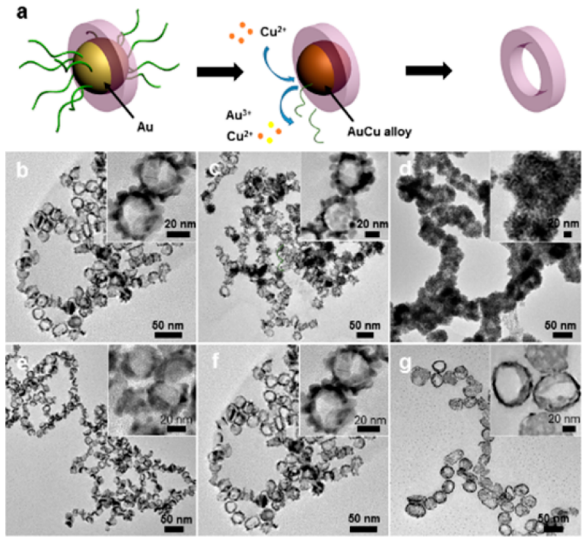

Figure 4. (a) Schematic diagram showing the formation of Pt NRs from Saturn-like Au–Pt NPs via the simultaneous alloying-etching mechanism. (b–d) TEM images of Pt NRs with different shell thickness: 4 nm (b), 10 nm (c), and 32 nm (d). (e–g) TEM images of Pt NRs with different inner diameter: 15 nm (e), 20 nm (f), and 30 nm (g).

ORR was used as a model reaction to compare the catalytic properties of NTs and NRs. Pt NTs and NRs with the thinnest shell (2 nm for NTs and 4 nm for NRs) were employed as nanocatalysts and compared to a commercial 5 nm Pt/C catalyst (Alfa Aesar). Electrochemical surface areas (ECSAs) were first estimated by integration of the under-potentially deposited hydrogen (H_{upd}) region of the cyclic voltammograms (Figure S16a). The NTs and NRs showed an ECSA of 34.18 $m^2\ g^{-1}_{pt}$ and 41.27 $m^2\ g^{-1}_{pt}$, respectively. The values are lower than those of reported 18.6 nm Pt nanocages[3] (46.8 $m^2\ g^{-1}_{Pt}$) and 20.1 nm Pt_3Ni nanoframes[4] (67.2 $m^2\ g^{-1}_{Pt}$) due to their larger dimensions. ORR was performed in O_2 saturated 0.1 M $HClO_4$ at a sweep rate of 20 mV/s. Compared with Pt/C, Pt NTs and NRs show a positive shift of 44 and 17 mV in half-wave potential in the ORR polarization curves (Figure S16b). This corresponds to a drastically enhanced specific activity of 1.48 and 0.52 mA cm^{-2} at 0.9 V (vs reversible hydrogen electrode, RHE) for the Pt NTs and NRs, respectively, compared to 0.26 mA cm^{-2} for the commercial Pt/C (Figure 5a). Moreover, the mass activity of Pt NTs and NRs was 0.54 and 0.21 A mg^{-1}_{Pt}, which was 3.6 and 1.7 times higher than that of Pt/C (Figure 5b). It is interesting to note that the NTs showed much better overall performance in ORR than NRs and other polycrystalline Pt hollow NPs,[32,33] although they have larger dimensions and same polycrystalline nature. The activity

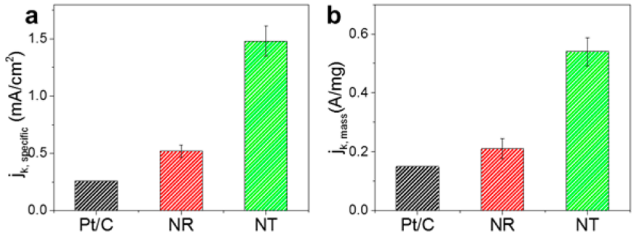

Figure 5. (a) Specific activities and (b) mass activities of Pt NTs and NRs relative to Pt/C at 0.9 V vs RHE.

DOI: 10.1021/jacs.6b01328
J. Am. Chem. Soc. 2016, 138, 6332–6335

is even close to that of recently reported Pt nanocages with well-defined facets (1.98 mA cm^{-2}, 0.75 A mg^{-1}_{Pt}).[3] This can be attributed to the unique tubular structure that allows the existence of some extended Pt surfaces with intrinsically high ORR specific activities on the side walls, which lead to dramatically enhanced overall ORR performance. Although the activity of our NTs is still lower than that of nanoframes made of Pt-based alloys,[4] we believe it can be further improved by careful facet control and alloying with other metals.[3,4]

In summary, we have developed a novel etching technique based on a unique simultaneous alloying−etching process for eliminating noble metals such as Au and Pd in organic solvent. This approach was demonstrated for the synthesis of sub-50 nm Pt NTs and NRs with controllable inner diameter and wall thickness. The Pt NTs with ultrathin wall exhibited superior catalytic activity for the ORR which could be attributed to the unique tubular feature. This synthetic strategy can be potentially extended for the synthesis of NTs with other different compositions (e.g., oxides). Moreover, the etching technique also paves a new route to carving structurally complex inorganic nanostructures with diverse applications in such as catalysis, energy storage, and biomedicine.

■ ASSOCIATED CONTENT

Supporting Information

The Supporting Information is available free of charge on the ACS Publications website at DOI: 10.1021/jacs.6b01328.

Experiments and characterization (PDF)

■ AUTHOR INFORMATION

Corresponding Authors

*jlgong@tju.edu.cn

*znie@umd.edu

Notes

The authors declare no competing financial interest.

■ ACKNOWLEDGMENTS

Z.N. gratefully acknowledges the financial support of National Science Foundation Career Award (DMR-1255377), National Science Foundation (CHE-1505839), 3M Non-tenured Faculty Award and Startup fund from the University of Maryland. J.G. thanks National Science Foundation of China (21222604, U1463205, and 21525626), the Program of Introducing Talents of Discipline to Universities (B06006), and the Program for New Century Excellent Talents in University (NCET-10-0611). D.R. and C.W. thank the support by the National Science Foundation (CHE-1437396). We also acknowledge the support of the Maryland NanoCenter and its NispLab. The NispLab is supported in part by the NSF as a MRSEC Shared Experimental Facilities.

■ REFERENCES

(1) Lou, X. W.; Archer, L. A.; Yang, Z. *Adv. Mater.* **2008**, *20*, 3987.

(2) Sun, Y.; Mayers, B.; Xia, Y. *Adv. Mater.* **2003**, *15*, 641.

(3) Zhang, L.; Roling, L. T.; Wang, X.; Vara, M.; Chi, M.; Liu, J.; Choi, S.-I.; Park, J.; Herron, J. A.; Xie, Z.; Mavrikakis, M.; Xia, Y. *Science* **2015**, *349*, 412.

(4) Chen, C.; Kang, Y.; Huo, Z.; Zhu, Z.; Huang, W.; Xin, H. L.; Snyder, J. D.; Li, D.; Herron, J. A.; Mavrikakis, M.; Chi, M.; More, K. L.; Li, Y.; Markovic, N. M.; Somorjai, G. A.; Yang, P.; Stamenkovic, V. R. *Science* **2014**, *343*, 1339.

(5) Kim, S.-W.; Kim, M.; Lee, W. Y.; Hyeon, T. J. *J. Am. Chem. Soc.* **2002**, *124*, 7642.

(6) Wirtz, M.; Parker, M.; Kobayashi, Y.; Martin, C. R. *Chem. - Eur. J.* **2002**, *8*, 3572.

(7) An, K.; Hyeon, T. *Nano Today* **2009**, *4*, 359.

(8) Yavuz, M. S.; Cheng, Y.; Chen, J.; Cobley, C. M.; Zhang, Q.; Rycenga, M.; Xie, J.; Kim, C.; Song, K. H.; Schwartz, A. G.; Wang, L. V.; Xia, Y. *Nat. Mater.* **2009**, *8*, 935.

(9) Sun, Y.; Xia, Y. *Science* **2002**, *298*, 2176.

(10) Métraux, G. S.; Cao, Y. C.; Jin, R.; Mirkin, C. A. *Nano Lett.* **2003**, *3*, 519.

(11) González, E.; Arbiol, J.; Puntes, V. F. *Science* **2011**, *334*, 1377.

(12) Jana, S.; Chang, J. W.; Rioux, R. M. *Nano Lett.* **2013**, *13*, 3618.

(13) McEachran, M.; Keogh, D.; Pietrobon, B.; Cathcart, N.; Gourevich, I.; Coombs, N.; Kitaev, V. *J. Am. Chem. Soc.* **2011**, *133*, 8066.

(14) Zhang, Q.; Wang, W.; Goebl, J.; Yin, Y. *Nano Today* **2009**, *4*, 494.

(15) Goldberger, J.; Fan, R.; Yang, P. *Acc. Chem. Res.* **2006**, *39*, 239.

(16) Sanchez-Castillo, M. A.; Couto, C.; Kim, W. B.; Dumesic, J. A. *Angew. Chem. Int. Ed.* **2004**, *43*, 1140.

(17) Gao, W.; Sattayasamitsathit, S.; Orozco, J.; Wang, J. *J. Am. Chem. Soc.* **2011**, *133*, 11862.

(18) Lee, W.; Scholz, R.; Nielsch, K.; Gösele, U. *Angew. Chem. Int. Ed.* **2005**, *44*, 6050.

(19) Manesh, K. M.; Cardona, M.; Yuan, R.; Clark, M.; Kagan, D.; Balasubramanian, S.; Wang, J. *ACS Nano* **2010**, *4*, 1799.

(20) Mayers, B.; Jiang, X.; Sunderland, D.; Cattle, B.; Xia, Y. *J. Am. Chem. Soc.* **2003**, *125*, 13364.

(21) Kijima, T.; Yoshimura, T.; Uota, M.; Ikeda, T.; Fujikawa, D.; Mouri, S.; Uoyama, S. *Angew. Chem. Int. Ed.* **2004**, *43*, 228.

(22) Huang, Z.; Liu, Y.; Zhang, Q.; Chang, X.; Li, A.; Yi, C.; Yang, Y.; Deng, L.; Khashab, N. M.; Gong, J.; Nie, Z. *Nat. Commun.* **2016**, submitted for publication.

(23) Nie, Z.; Fava, D.; Kumacheva, E.; Zou, S.; Walker, G. C.; Rubinstein, M. *Nat. Mater.* **2007**, *6*, 609.

(24) Wen, T.; Zhang, H.; Tang, X.; Chu, W.; Liu, W.; Ji, Y.; Hu, Z.; Hou, S.; Hu, X.; Wu, X. *J. Phys. Chem. C* **2013**, *117*, 25769.

(25) Sánchez-Iglesias, A.; Pastoriza-Santos, I.; Pérez-Juste, J.; Rodríguez-González, B.; García de Abajo, F. J.; Liz-Marzán, L. M. *Adv. Mater.* **2006**, *18*, 2529.

(26) Pastoriza-Santos, I.; Liz-Marzán, L. M. *Nano Lett.* **2002**, *2*, 903.

(27) Chen, W.; Yu, R.; Li, L.; Wang, A.; Peng, Q.; Li, Y. *Angew. Chem.* **2010**, *122*, 2979.

(28) Xu, Z.; Lai, E.; Shao-Horn, Y.; Hamad-Schifferli, K. *Chem. Commun.* **2012**, *48*, 5626.

(29) Sreeprasad, T. S.; Samal, A. K.; Pradeep, T. *Langmuir* **2007**, *23*, 9463.

(30) Kim, D.; Resasco, J.; Yu, Y.; Asiri, A. M.; Yang, P. *Nat. Commun.* **2014**, *5*, 4948.

(31) Lim, B.; Jiang, M.; Camargo, P. H. C.; Cho, E. C.; Tao, J.; Lu, X.; Zhu, Y.; Xia, Y. *Science* **2009**, *324*, 1302.

(32) Chen, H. M.; Liu, R.-S.; Lo, M.-Y.; Chang, S.-C.; Tsai, L.-D.; Peng, Y.-M.; Lee, J.-F. *J. Phys. Chem. C* **2008**, *112*, 7522.

(33) Peng, Z.; Wu, J.; Yang, H. *Chem. Mater.* **2010**, *22*, 1098.

(34) Stamenkovic, V. R.; Mun, B. S.; Arenz, M.; Mayrhofer, K. J. J.; Lucas, C. A.; Wang, G.; Ross, P. N.; Markovic, N. M. *Nat. Mater.* **2007**, *6*, 241.

DOI: 10.1021/jacs.6b01328
J. Am. Chem. Soc. 2016, 138, 6332−6335